www.lajss.org
Latin American Journal of Solids and Structures 4 (2007) 315–330

Bending of floating wedges with initial curvature under deformation dependent loading

João B. de Aguiar*

Sistemas Mecânicos, Escola Politécnica, USP – Brazil

Abstract

The bending moment distribution of beams of variable width, with initial curvature, while resting on a linear elastic foundation, loaded by in-plane as well as out-of-plane resultants is formulated. A numerical procedure is developed to generate the solution of the two point boundary value problem. As interface loading is deformation dependent, an iterative procedure is devised to obtain the correct loads. A specific case is analyzed and its bending field presented. Dependence with respect to the interface variables, wedge angle and imperfection profile is considered. Comparison to the uniform beam case is also performed. While initial curvature has limited effects on bending moments, wedging has dramatic effects, decreasing overall values dramatically.

Keywords: wedge beams, curved beams, elastic foundation, numerical solution, bending field

1 Introduction

Wedge type modeling occurs in several fields of engineering, like geology, structures and ice mechanics. In the last case, in particular, it has attracted lots of attention in what concerns impact to an offshore facility as ice floes are really irregular and many times with an increasingly larger width. Or it may well be that the model is used to capture the post radial cracking behavior of ice plates indented in the contact with inclined walls [7]. In any case a complete description of this kind of problem, whose loading is deformation dependent, and deals with a semi-infinite field, is hard to attain with finite element techniques.

Techniques used in this context consider several simplifications, including use of ice sheets, of rectangular form, supported by springs to model foundation effect, and held far away from the contact interface as in [5]. Loading may be of the displacement or point force boundary type. Wedging geometry of ice caused by radial and circumferential cracks during deformation may then be mapped. An alternative to this procedure includes use of semi-infinite elements, as in Abaqus program [2] or lattice models [12]. But initial curvature and thickness variations are not considered. In the last case use of an effective bearing band is proposed [13], but this solution does not eliminate the problem concerning changes of the equal area axis, caused by

*Corresp. author email: jbaguiar@usp.br Received 29 Nov 2006; In revised form 21 Oct 2007

thickness variations, and therefore the curvature of this axis. Or if not, changes of strength through thickness on its own.

Particular way an ice floe geometry changes has been considered under the diverse points of view, included the dynamic one [10]. Starting from a perfect ice formation, driven by wind, currents and waves, a model is constructed to show how impact, lateral and frontal, builds thickness variations in the ice floe. These variations result, unless a symmetrical profile is considered, in a curved equal area axis. Ridges and consolidated rubbles complete the panorama [3, 4].

Here it is developed a numerical scheme of solution that can be used with many descriptions of width variation. This scheme allows the choosing of the width variation profile, and the solution is attained by means of an iterative process in a two-point boundary value problem. Initial curvature of the beam, occurring at the cause of natural conditions, or caused by past events, may have a geometric or material character. Profile variations are complex, but they may be built from series algebra of harmonic functions used here.

Analysis of the contact interaction with inclined walls shows loading to be deformation dependent. This correction is taken into account. Particular dependence on the boundary terms, b.t., wedge angle and initial curvature is looked upon. Results show the bending field to be very affected by wedge angle, and to a lesser degree by initial curvature, that controls most the position of point of maximum, not its value. In the end, by using Taylor expansion, it is shown how to add up these effects to the close form solution of the uniform beam, so as to estimate the behavior of the wedge.

2 Modeling

2.1 Element equilibrium

The pair of differential equations of equilibrium of a beam element constituted by an homogeneous elastic material, identified by the pair $< E, \nu >$, with constant thickness h_0, variable width $b = \omega\, b_0$, and initial curvature described by a profile function w_i, while resting on a linear elastic foundation of constant γ_{sw}, Fig. 1, will be [11]:

$$\begin{aligned} &\partial_y N \cong 0 \\ &\partial_{yy}[E'I\partial_{yy}(w)] - \partial_y[N\partial_y(w + w_i)] + b\gamma_{sw} w \cong 0; \qquad \partial_y = \tfrac{d}{dy} \end{aligned} \tag{1}$$

The first of these equations refers to in-plane conditions, whereas the second considers the out-of-plane ones. Quasi-static conditions of loading along with initial curvature of the equal area axis are admitted. Reason for this particular modeling choice lies in the characteristics of the early winter impact-failure scenario of brittle ice.

Combination of these equations into a single statement gives:

$$\partial_{yy}[\omega\partial_{yy}(w)] + 4\gamma_0^4\partial_{yy}(w) + 4\delta_0^4\omega\, w = -4\gamma_0^4\partial_{yy}(w_i) \tag{2}$$

which depends on the coefficients,

$$\gamma_0 = (\frac{n_0}{4E'i_0})^{\frac{1}{4}}; \qquad n_0 \geq 0 \quad ; \quad \delta_0 = (\frac{\gamma_{sw}}{4E'i_0})^{\frac{1}{4}}; \tag{3}$$

In these $n_0 = \frac{N_0}{b_0}$ is the value of the normal force per unit width b_0 at the origin. Function ω is a width-variation multiplicative function that measures the variations of width b with respect to the origin width b_0. The second moment of inertia per unit width is $i_0 = {}^{I_0}/_{b_0}$ and E' is the equivalent beam Young's modulus and γ_{sw} is the mass density of salt water. So,

$$i_0 = \frac{h_0^3}{12}; \qquad E' = \frac{E}{(1-\nu^2)} \tag{4}$$

Here E is the elastic modulus of the material and ν its Poisson's ratio, introduced to allow modeling of wide beams as well as strips with due care of proper choice of value.

2.2 End conditions

For the case where the beam is loaded at the origin by a shear force and a bending moment, as occurs when an inertia driven ice floe hits a fixed offshore platform wall, loading introduced by the contact at this end may be described by

$$\begin{array}{ll} y = 0; & m_0 = -E'i_0\omega_0\partial_{yy}(w)_0 \\ & v_0 = -E'i_0\omega_0\partial_{yyy}(w)_0 - n_0\partial_y(w+w_i)_0 + \frac{\partial_y(\omega)_0}{\omega_0}m_0 \end{array} \quad . \tag{5}$$

These equations relay on the free parameter n_0, related to the solution of the in-plane problem. They also reveal dependence upon the deformation of the beam at the origin. At the other end, the far end, regularity conditions apply.

$$\begin{array}{ll} y = L; & w_L \leq K_w \\ & \partial_y(w)_L \leq K_\theta \end{array} \tag{6}$$

where $< K_w, K_\theta >$are suitable small constants. Here the subscripts are employed to describe the position where the variable should be computed. Hence, for the semi-infinite body, for example, setting $L \to \infty$ is mandatory.

2.3 System of equations

Solution of the fourth order differential equation of equilibrium shown above, subjected to the stated boundary conditions, may be accomplished by a transformation of this equation into a set of four linear equations, as it includes derivatives up to this order. A transformation of the boundary conditions has to be performed as well. Let $\mathbf{u}$ be the vector:

$$\lfloor u \rfloor = \lfloor \ (w) \quad \partial_y(w) \quad \partial_{yy}(w) \quad \partial_{yyy}(w) \ \rfloor; \quad w = w(y; b.t.; \theta_0, \omega_0; w_i) \tag{7}$$

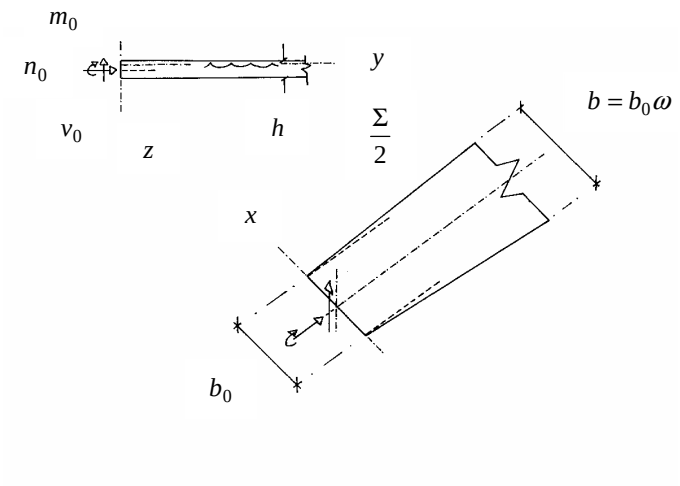

Figure 1: Variable width ice floe impact scenario.

where b.t. stands for the boundary terms $< n_0, m_0, v_0 >$. Here the row representation form is employed. To this kind of dependence, interface rotation $\theta_0 = \partial_y(w)_0$ is added. And this allows Eq. (2) to be rewritten in the form:

$$\{u'\} = [K]\{u\} + \{u_i\}\,; \qquad u'_l = \partial_y(u_l); \qquad l = 1,2,3,4 \tag{8}$$

where the matrix $[K]$ comprises the elements,

$$[K] = \begin{bmatrix} 0 & 1 & 0 & 0 \\ 0 & 0 & 1 & 0 \\ 0 & 0 & 0 & 1 \\ -4\delta_0^4 & 0 & -\frac{\partial_{yy}(\omega)+4\gamma_0^4}{\omega} & -\frac{2\partial_y(\omega)}{\omega} \end{bmatrix} \quad ; \quad \{u_i\} = \begin{Bmatrix} 0 \\ 0 \\ 0 \\ -\frac{4\gamma_0^4}{\omega}\partial_{yy}(w_i) \end{Bmatrix}. \tag{9}$$

The set of boundary conditions, on the other hand, considered the proper equivalent form, follows from Eqs. (5) and (6) and can be cast into the form:

$$\{\varphi\} = [A]\{u_0\} + [B]\{u_L\} + \{\alpha\} - \{\beta\}\,; \qquad \{\varphi\} = \{0\} \tag{10}$$

where the matrices $[A]$ and $[B]$ are such that:

$$[A] = \begin{bmatrix} 0 & 0 & 0 & 0 \\ 0 & 0 & 0 & 0 \\ 0 & 0 & E'i_0\omega_0 & 0 \\ 0 & n_0 & 0 & E'i_0\omega_0 \end{bmatrix}; \qquad [B] = \begin{bmatrix} 1 & 0 & 0 & 0 \\ 0 & 1 & 0 & 0 \\ 0 & 0 & 0 & 0 \\ 0 & 0 & 0 & 0 \end{bmatrix} \tag{11}$$

whereas the vector $\{\alpha\}$, in row form, will be:

$$\lfloor \alpha \rfloor = \left\lfloor 0 \quad 0 \quad m_0 \quad -\frac{\partial_y(\omega)_0}{\omega_0}m_0 + v_0 \right\rfloor \quad \lfloor \beta \rfloor = \lfloor \; K_w \quad K_\theta \quad 0 \quad -n_0\partial_y(w_i)_0 \; \rfloor \tag{12}$$

which then completes the system of equations to be solved.

2.4 Numerical solution

Solution of the above system depends, for every value of n_0, on the determination of the exact $\{u\}$ vector that makes $\{\varphi\}$ null for specified values of the left and right end vectors. It should be kept in mind, however, that in general these values may depend upon the behavior of the beam, and as such are not exactly known a priori. A numerical trial and error type of approach may then be applied, using a Newton scheme of solution. Specifically: trial vectors are chosen to set conditions at the left end of the interval [0, L). This is a subset in the vector space as some of the components at the origin vector are free. It comprises an iteration sequence intended the matching of the correct boundary conditions at the other end of the beam [6].

Hence, in the iterative process, if at iteration j, of a series of M trials,

$$\{\varphi^j\} \neq \{0\}; \qquad \{\varphi^j\} = [A]\{u_0^j\} + [B]\{u_N^j\} + \{\alpha^j\} - \{\beta^j\}; \qquad j = 1, 2, ..., M \tag{13}$$

over a discretized space containing $N+1$ stations, $\{y_l\};\ l = 0, 1, 2, ..., N$, being

$$\{u_0^j\} = \{u^j(y_0)\}; \qquad \{u_N^j\} = \{u^j(y_N)\}; \quad y_0 = 0; \quad y_N = L; \quad \forall j \tag{14}$$

then requiring that the boundary conditions in the next iteration are met is equivalent to asking for an increment that makes:

$$\{\varphi^{j+1}\} = \{0\}; \qquad \{\varphi^{j+1}\} = [A]\{u_0^{j+1}\} + [B]\{u_N^{j+1}\} + \{\alpha^{j+1}\} - \left\{\beta^{j+1}\right\} \tag{15}$$

being $\Delta\{u_0^j\}$ the required vector increment. If this is so, then

$$\left\lfloor \partial_{\{u_0^{j+1}\}}\{\varphi^{j+1}\} \right\rfloor \Delta\{u_0^j\} = -\{\varphi^j\}; \qquad \Delta\{u_0^j\} = \{u_0^{j+1}\} - \{u_0^j\} \tag{16}$$

where, from Eq. (15), the partial derivative with respect to the trial vector is

$$[\partial_{\{u_0^{j+1}\}}\{\varphi^{j+1}\}] = [A][I] + [B][\partial_{\{u_0^{j+1}\}}\{u_N^{j+1}\}] + [\partial_{\{u_0^{j+1}\}}\{\alpha^{j+1}\}] - [\partial_{\left\{u_0^{j+1}\right\}}\left\{\beta^{j+1}\right\}] \tag{17}$$

being:

$$[\partial_{\{u_0^{j+1}\}}\{u_N^{j+1}\}] = [\partial_{\{u_{N-1}^{j+1}\}}\{u_N^{j+1}\}]\,[\partial_{\{u_{N-2}^{j+1}\}}\{u_{N-1}^{j+1}\}]...[\partial_{\{u_1^{j+1}\}}\{u_2^{j+1}\}]\,[\partial_{\{u_0^{j+1}\}}\{u_1^{j+1}\}] \tag{18}$$

which then requires a Taylor expansion to relate the derivatives

$$\{u'^{j+1}_{l+1}\} = \{u'^{j+1}_{l}\} + \partial_y\{u'^{j+1}_{l+1}\}\Delta y; \quad \{u'^{j+1}_{l+1}\} = [K_{l+1}]\{u_{l+1}^{j+1}\} + \{u_i^{j+1}\}; \qquad [K_{l+1}] = [K(y_{l+1})] \tag{19}$$

Finally combination of this result with that of Eq. (17) produces

$$\{u_{l+1}^{j+1}\} = [T_l^{l+1}]\{u_l^{j+1}\}; \qquad [T_l^{l+1}] = [M_{l+1}^{-1}][K_l] \tag{20}$$

result that relates vectors at successive stations. In it the section matrix

$$[M_{l+1}] = ([I] - \Delta y[K'_{l+1}]\,[K^{-1}_{l+1}] - \Delta y[K_{l+1}])\,[K_{l+1}]; \qquad [K'_{l+1}] = \partial_y[K_{l+1}] \tag{21}$$

appears in its inverse form. This form depends on parameters of the medium, sectional properties, loading as well as material variables. Complete transfer matrix from start to last section may be displayed as the product

$$[T^N_0] = \prod_{l=0}^{N-1} [T^{l+1}_l]; \tag{22}$$

whose coefficients are polynomial expressions of the discretization step. The matrix $\mathbf{T}^{l+1}_l$does not depend upon the iteration being executed. Once this transfer matrix is computed, for the iteration in case, the Jacobian, Eq. (17), can be directly calculated

$$[J^{j+1}] = [A]\,[I] + [B]\,[T^N_0] + \frac{\partial(\{\alpha^{j+1}\} - \{\beta^{j+1}\})}{\partial\{u^{j+1}_0\}} \tag{23}$$

which allows the calculation of an increment $\Delta\{u^j_0\}$, Eq. (16).

3 Application

3.1 Loading

When the ice floe, driven by currents and wind, is loaded during contact with the inclined wall of an offshore platform, quasi-static conditions are approached with loading coming from the impulse generated by the inertia change of the ice. Flexure, shear and compression at the interface are produced, with the rate of change of the linear momentum $\mathbf{l}$ equaling the sum of the external forces, normal and shear, per unit width at the interface:

$$\Delta\mathbf{l} = \mathbf{i}; \quad \mathbf{l} = \int_{\mathbf{0}}^{\infty} \mathbf{v}\frac{\gamma_i}{g}\omega\, h_0 dy; \quad \mathbf{i} = \int_{0}^{\mathbf{t}} (\mathbf{n_0} - \mathbf{v_0})dt \qquad \dot{\mathbf{l}} = \mathbf{n_0} - \mathbf{v_0} \tag{24}$$

while the rate of change of the angular momentum $\mathbf{a}$ equals the resultant interface moment $\mathbf{m}_0$:

$$\Delta\mathbf{a} = \mathbf{h}; \quad \mathbf{a} = \int_{\mathbf{0}}^{\infty} \mathbf{\Omega}\frac{\gamma_i}{g}\omega\, i_0 dy; \quad \mathbf{h} = \int_{\mathbf{0}}^{\mathbf{t}} \mathbf{m_0} dt; \qquad \dot{\mathbf{a}} = -\mathbf{m_0} \tag{25}$$

both expressions dependent on linear $\mathbf{v}$ and angular Ω velocities, being γ_i the specific weight of the ice, and g the gravity acceleration. Added mass factors could be incorporated as well [8].

Values of normal n_0, bending moment m_0 and shear force v_0 at the interface depend on the contact between platform and beam. They are resultants that may be described by the

coefficient of friction μ between ice and the rigid wall of the platform, its slope angle ϕ and the coefficient of eccentricity ζ, Figs. 2 and 3. Solving the normal $r_0\mathbf{e}_n$ and tangential $\mu r_0\mathbf{e_t}$ to the inclined wall in terms of its horizontal and vertical components

$$z_0 = r_0(\cos\phi^u - \mu\sin\phi^u); \qquad y_0 = r_0(\sin\phi^u + \mu\cos\phi^u) \tag{26}$$

for the upper slope case, and denoting the rotation at the origin by θ_0 leads to:

$$n_0 = -z_0\sin\theta_0 + y_0\cos\theta_0; \quad v_0 = z_0\cos\theta_0 + y_0\sin\theta_0; \quad m_0 = -n_0 e \tag{27}$$

being $e = \zeta h_0; -0.5 \leq \zeta \leq 0.5$ the eccentricity. The coefficient μ depends on the existence of sliding or sticking contact conditions, for every value of r_0. An additional consideration has to be introduced here, as the shear force at the origin v_0 will also depend on the direction of the motion of the beam. For the riding-up condition, or up-slope case, under slipping and sticking stages,

$$\begin{array}{lll} v_0^u \leq n_0\tan(\phi_t^u); & \phi_t^u \leq \rho & \\ v_0^u = n_0\tan(\phi_t^u - \rho); & \phi_t^u \geq \rho & \phi_t^u = \phi^u + \theta_0 \end{array} \tag{28}$$

where $\rho = \tan^{-1}(\mu)$ is a material parameter, related to the way the ice and wall interact, and dependent on surface roughness and temperature among other factors. Notice that deformation of the beam acts to create an effective value of friction angle.

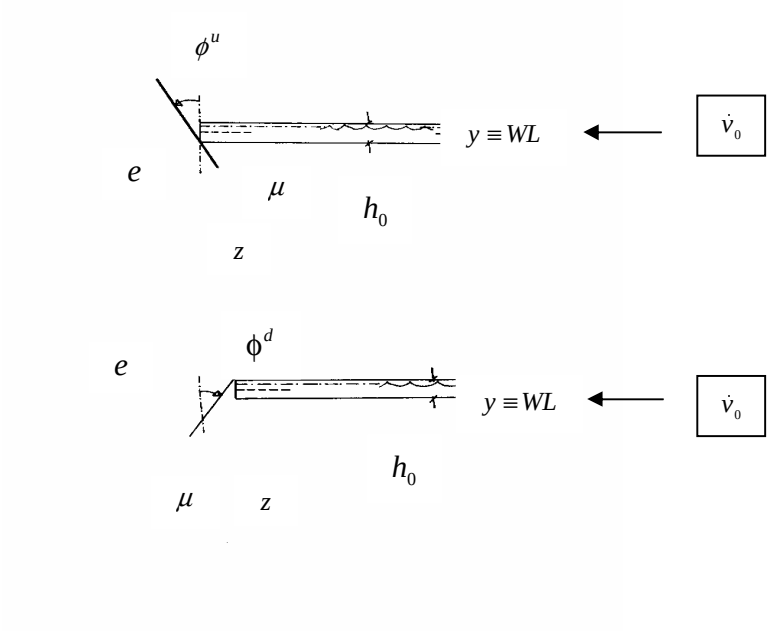

Figure 2: Up-slope and down-slope configurations for initial contact condition.

Down-slope case, on the other hand, would derive from a slope angle ϕ^d, and result in a shear force $v_0^d = -v_0^u$ and bending moments $m_0^d = -m_0^u$ for the same normal n_0 and same absolute values of slope angle, eccentricity and coefficient of friction. Table 1 presents the values considered in the present analysis.

Table 1: Boundary terms used in the analysis.

Loading Parameters	
Slope angle set, degrees	$\phi = \{15, 30, 45\}$
Eccentricity set	$\zeta = \{-0.5, 0, 0.5\}$
Friction coefficient set	$\mu = \{0.05, 0.25\}$

3.2 Material parameters

Ice is a very complex material whose constitutive equation depends on the type of microstructure considered, time of the year, form of response sought, etc. For ice features in a brittle state, in salt water, Table 2 presents some average values of the properties of this material [9]. Foundation constant, salt water in this case, is taken to be $\gamma_{sw} = 1.0045e + 4\text{Pa/m}$.

Table 2: Some properties of the beam material.

Properties of Ice	
Elastic modulus, Pa	$E = 0.50e + 10$
Poisson's ratio	$\nu = 0.30$
Flexural strength, MPa	$S_f = 0.70$
Compressive strength, MPa	$S_c = 5.0$

3.3 Interface rotation

In the field, the monitored variable r_0, the intensity of contact, has to be used to compute the interface normal n_0. However, because the displacements do depend on the interface conditions, loading at origin is related to the rotation θ_0, Eqs. (10)-(12) and (27),

$$\frac{\partial \left\{\alpha^{j+1}\right\}}{\partial \left\{u_0^{j+1}\right\}} = \begin{bmatrix} 0 & 0 & 0 & 0 \\ 0 & 0 & 0 & 0 \\ 0 & 0 & \partial_{\theta_0^{j+1}}(m_0^{j+1}) & 0 \\ 0 & \partial_{\theta_0^{j+1}}[v_0^{j+1} - m_0^{j+1}(\frac{\partial_y \omega_0}{\omega_0})] & 0 & 0 \end{bmatrix} \tag{29}$$

where,

$$\frac{\partial m_0^{j+1}}{\partial \theta_0^{j+1}} = -r_0 e\{\cos(\phi)[\mu\cos(\theta_0^{j+1}) - \sin(\theta_0^{j+1})] - \sin(\phi)[\cos(\theta_0^{j+1}) - \mu\sin(\theta_0^{j+1})]\} \tag{30}$$

and,

$$\frac{\partial v_0^{j+1}}{\partial \theta_0^{j+1}} = r_0\{\cos(\phi)[\cos(\theta_0^{j+1}) + \mu\sin(\theta_0^{j+1})] + \sin(\phi)[-\sin(\theta_0^{j+1}) + \mu\cos(\theta_0^{j+1})]\} \tag{31}$$

Moreover, from Eq. (27),

$$\frac{\partial\{\beta^{j+1}\}}{\partial\{u_0^{j+1}\}} = \begin{bmatrix} 0 & 0 & 0 & 0 \\ 0 & 0 & 0 & 0 \\ 0 & 0 & 0 & 0 \\ 0 & -\frac{\partial n_0^{j+1}}{\partial \theta_0^{j+1}}\partial_{,y}(w_i)_0 & 0 & 0 \end{bmatrix} \tag{32}$$

where the rotation correction for the normal comes from:

$$\frac{\partial n_0^{j+1}}{\partial \theta_0^{j+1}} = -\frac{1}{e}\frac{\partial m_0^{j+1}}{\partial \theta_0^{j+1}} \tag{33}$$

Therefore guessing the entrance values for the u_0^{j+1} vector requires that the curvature $\kappa_0^{j+1} = \partial_{,yy}(w^{j+1})_0$ be such that $\kappa_0^{j+1} = -\frac{m_0^{j+1}}{E'i_0}$, where m_0^{j+1} does depend on the guessed value of θ_0^{j+1}, according to the above, and it does not represent a free choice. The same can be said of the rate of curvature at the origin, $\partial_{,y}(\kappa^{j+1})_0$, that should obey the equation for shear force at the interface, Eq. (5).

3.4 Geometry

Solution developed above was implemented for some specific beam geometries and the results presented in graphic form for the internal bending moment $m = -E'i_0\omega\partial_{,yy}(w)$ under different amounts of initial curvature, and wedge angle Σ. The particular solution to Eq. (2) will depend on the type of function w_i chosen to represent the profile of initial imperfection of the axis of the beam. For harmonic-type imperfection profiles:

$$w_i = a_i\sin(\kappa_i y + \psi_i) \tag{34}$$

where a_i is the amplitude of the sinusoidal, considered constant, $\kappa_i = {}^{2\pi}/_{\lambda_i}$ is a wave-number-like parameter, being λ_i the associated wave-length, and ψ_i some phase angle, Fig. 4. Imperfection profiles for the equal area axis used in the analysis are shown in Table 3. Aspect ratio of the beams at origin was taken as ${}^{h_0}/_{b_0} = \{1, 2, 4\}$. Wedge description followed a linear, symmetric, distribution starting at the loading interface, with total wedge angle Σ:

$$\omega = 1 + 2\,tg(\frac{\Sigma}{2})\left[\frac{y}{b_0}\right] \tag{35}$$

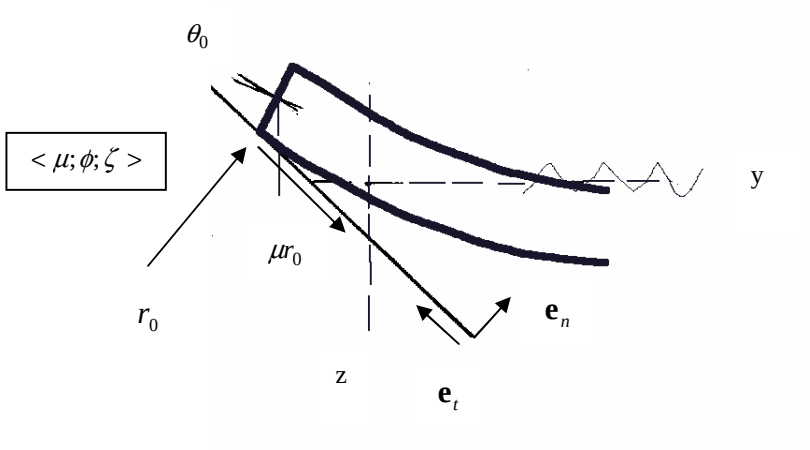

Figure 3: Point contact scenario at interface of irregular beam.

Table 3: Set of profile parameters used in the analysis.

Initial Curvature and Wedge Variables
Amplitude Ratio $\frac{a_i}{h_0} = \{0, 0.125, 0.250\}$
Wave-length Ratio $\frac{\lambda_i}{\lambda_0} = \{0.125, 0.250, 0.500, \rightarrow \infty\}$
Phase angle [deg] $\psi_i = \{0, 45, 90, 180, 270\}$
Wedge angle [deg} $\Sigma = \{0.0, 7.5, 15., 22, 5\}$

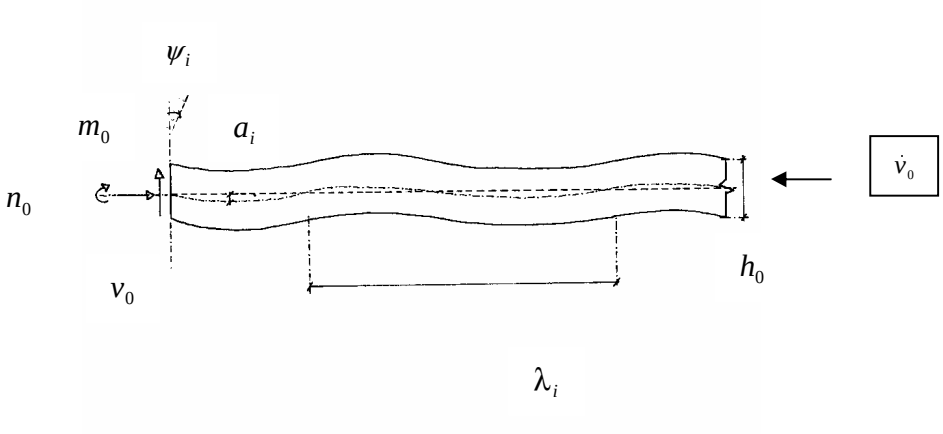

Figure 4: Initial curvature profile.

4 Bending moment distribution

The effect of the wedge angle Σ on the distribution of bending moment m along variable width beams, with initial curvature w_i written in vector form, is presented in the plot of Fig. 5. It is obtained from the third entrance to the vector $\mathbf{u}$, Eq. (7), through the curvature $\partial_{yy}(w)$:

$$m = \widehat{m}_{\Sigma}(y; b.t; \{w_i\}; \Sigma); \quad m = -E' i_0 \omega \partial_{yy}(w); \quad \lfloor w_i \rfloor = \begin{bmatrix} a_i & \kappa_i & \lambda_i \end{bmatrix} \tag{36}$$

being non-dimensional ordinates constructed from the failure bending moment $m_f = \frac{2 i_0 S_f}{h_0}$, and non-dimensional abscissas from reference to the wave-like number $\lambda_0 = \frac{2\pi}{\delta_0}$. Material parameters were the ones indicated in Table 2. Loading is set according to the values: $\xi = 0.50$,$\phi = 30^0$; $\mu = 0.05$ and $\frac{n_0}{n_c} = 0.001$. Aspect ratio $\frac{h_0}{b_0} = 2.$ at the origin is chosen.

Overall, it is observed a decrease on the peak bending moment $m_e = \widehat{m}_e(\Sigma)$ as the wedge angles are increased, and all other variables kept constant. At the same time the point of its occurrence $y_e = \widehat{y}_e(\Sigma)$ draws closer to the loading edge. This means that the size of the broken blocks get smaller and smaller as the beam gets wider and wider.

Points of occurrence of critical values of bending moment are therefore important. For different values of normal force, they occur when:

$$\partial_y(m) = 0; \tag{37}$$

what then requires a numerical procedure to be applied. Chosen an initial trial point, $y^{(j)} = y_e^{(j)}$ for the j-th trial, forward Newton-Raphson application will set an increment $\Delta y^{(j)}$ related to the Jacobian $J^{(j)} = \partial_{yy}(m)_{y^{(j)}}$ such that:

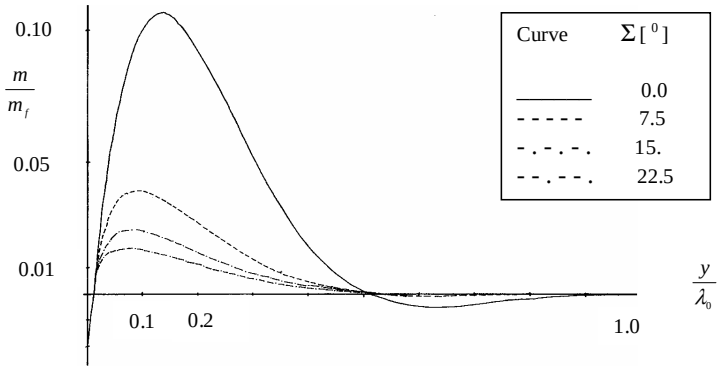

Figure 5: Plot of the dependence of bending moments upon the wedge angle.

$$\Delta y^{(j)} = -\partial_y(m)^{(j)} {J^{(j)}}^{-1}; \quad J^{(j)} \neq 0 \tag{38}$$

Furthermore, for small wedge angles and small initial curvatures, a Taylor expansion of the bending moment function m, Eq. (35), around the uniform beam profile, for different boundary configurations, may be obtained from:

$$m_\Sigma(y;b.t;\{w_i\};\Sigma) \cong m_\Sigma(y;b.t;w_i=0;\Sigma=0)+\partial_{,\Sigma}m(y;b.t;\{w_i\};\Sigma)\,{}_u\Sigma+\{\partial_{\{w_i\}}m(y;b.t;\{w_i\};\Sigma)_u\}\cdot\Delta\{w_i\} \tag{39}$$

where m for $\Sigma = 0$ and $\{w_i\} = \{0\}$ equals m_u, corresponding to the uniform beam, and whose expression is [1]:

$$m_u = -E'i_0 \exp(-\alpha y)[C_m \cos(\beta y) + S_m \sin(\beta y)] \tag{40}$$

with:

$$\begin{aligned} C_m &= (\alpha^2-\beta^2)C - 2\alpha\beta S \\ S_m &= 2\alpha\beta C + (\alpha^2-\beta^2)S \end{aligned} \tag{41}$$

being:

$$C = -2\frac{\beta(\alpha^2+\beta^2)m_0 + 2\alpha\beta v_0}{oE'i_0};\; S = 2\frac{\alpha(\alpha^2+\beta^2)m_0 + (\beta^2-\alpha^2)v_0}{oE'i_0} \tag{42}$$

being $\alpha = \sqrt{\delta_0^2 - \gamma_0^4}$ and $\beta = \sqrt{\delta_0^2 + \gamma_0^4}$ and $o = 2\beta\left(\alpha^2+\beta^2\right)\left(3\alpha^2-\beta^2\right)$. Therefore together with the wedge angle dependence, Fig. 5, entails estimates to be obtained fast. Boundary terms affect the bending behavior in different ways. Eccentricity of loading produces the dependency shown in Fig. 6, with increase of bending moments, in general, with positive values of ς.

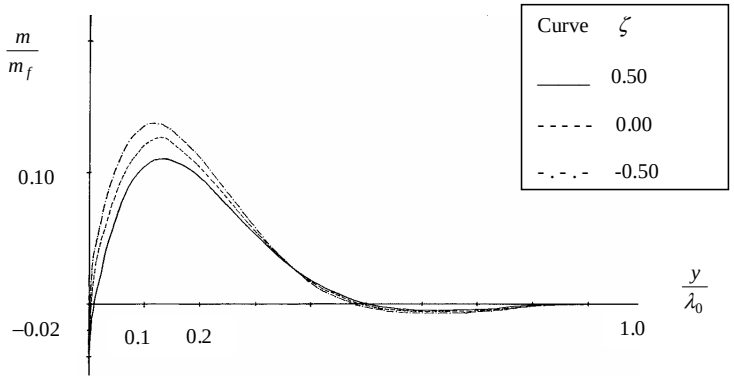

Figure 6: Plot of eccentricity of loading effect on bending moments for $\Sigma = 0$.

The slope angle effect is shown in Fig. 7. Here the steeper the wall, the higher the in-plane loads. As lower slopes are considered, lateral loads increase, and the problem is dominated by bending.

The coefficient of friction between the interacting surfaces, a line contact load for the ice strip that conducts to the undistributed overall terms $< n_0, m_0, v_0 >$, presents the effect depicted in Fig. 8. It shows increase of peak values of bending moment, with little position change, with increase of the coefficient of friction.

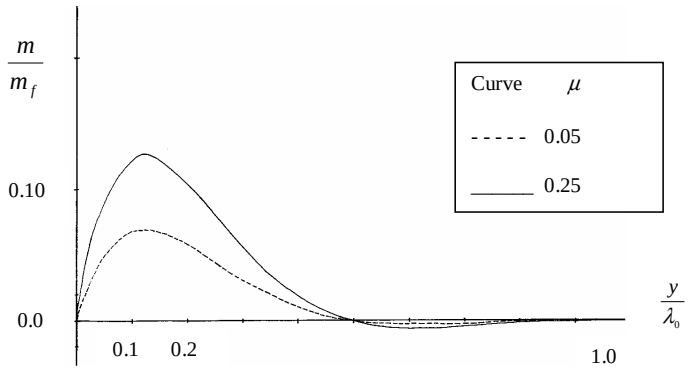

Figure 7: Plot of slope angle effect on bending moments for $\Sigma = 0$.

Presence of the initial curvature changes the bending moment distribution in different ways. Using the uniform beam as reference, Fig. 9 shows the dependence of bending moments with respect to amplitude of initial imperfections. The higher the amplitude of initial curvature a_i, the greater the change in maximum value of bending moment. For peak values it represents a decrease.

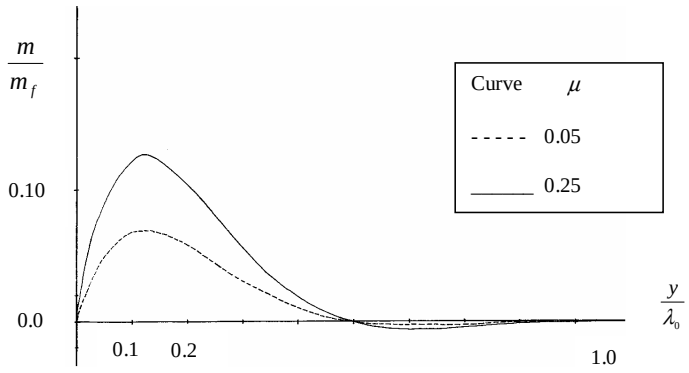

Figure 8: Plot of dependence of bending moments upon friction coefficient for $\Sigma = 0$.

In figures 10 and 11, wavelength λ_i and phase angles ψ_i are considered. These factors present a mixed effect, increasing and decreasing the bending moments. In a softer manner, as compared to the amplitude effect, as qualitatively the plots show.

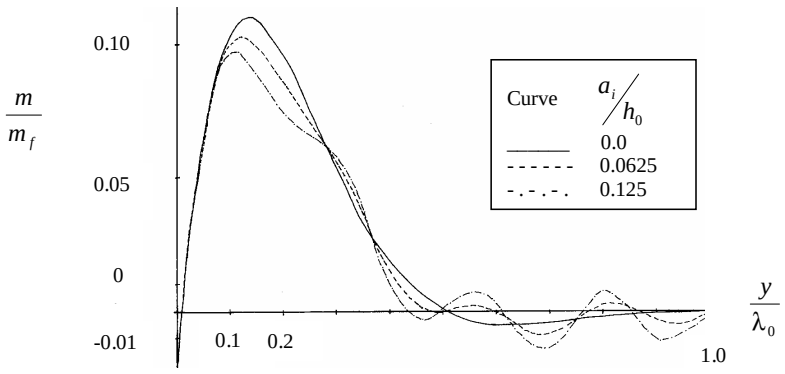

Figure 9: Initial curvature amplitude effect on bending moments for $\Sigma = 0$.

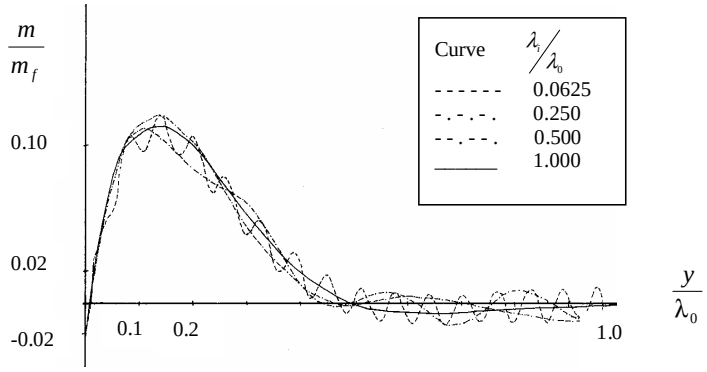

Figure 10: Effect of wave-length of imperfections on bending moments for $\Sigma = 0$.

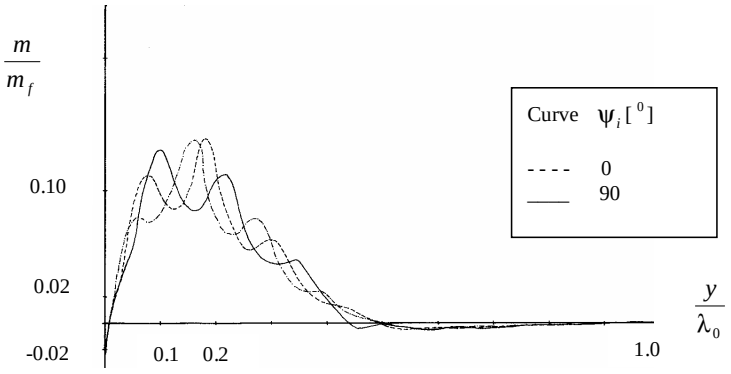

Figure 11: Effect of phase angle of imperfections on bending moments for $\Sigma = 0$.

5 Conclusions and extensions

The numerical scheme of solution presented here, coded and implemented using Fortran language, is very general and may be used with symmetric and unsymmetrical wedge profiles. In particular bi-linear forms of variation of width appear in many instances, and they can be addressed. Results above have shown the dramatic influence of wedging in the lowering of bending moments, and thus bending failure avoidance. Initial curvature has as a much lower importance in setting the peak values than it has in setting its position, and therefore size of broken blocks. It represents changes, in general, of the order of 20%, over the uniform beam case. Hence, much less than the wedge effect.

Characterization of the limits of the solution can be pursued with the inclusion of a failure criterion, using some damage parameter or a failure stress method, drawing the failure locus and then generating the set of failure loads for every configuration sought.

References

[1] J. B. De Aguiar. Displacement of semi-infinite beams on a elastic foundation under bending-compression loading. In *XVIII Congresso Brasileiro de Engenharia Mecânica, COBEM 05*, São Paulo, 2005.

[2] Hibbit, Karlson & Sorensen, Inc. *Abaqus Theory Manual*. 2002.

[3] http://en.tek.norut.no/norut_teknologi/forskning/konstruksjonsteknikk/ice_mechanics.

[4] http://www.hsva.de.

[5] M. J. Kaldjian. Ice-sheet failure against inclined and conical structures. *Computers and Structures*, 26(1-2):145–152, 1987.

[6] H. B. Keller. *Numerical Methods for Two-point Boundary Value Problems*. Gim-Blausdell, Waltham, MA., 1968.

[7] A. D. Kerr. The determination of horizontal forces that a floating ice plate exerts on a structure. *Journal of Glaciology*, 20(82), 1987.

[8] C. H. Luk. A flexural and longitudinal elastic wave propagation theory applied to ice floe impact with sloping structures. In 7^{th} *O.M.A.E.*, volume 109 (1), pages 75–84, 1987.

[9] M. Mellor. Mechanical behavior of sea ice. *Cold Regions Research and Engineering Laboratory, Monograph 83-1*, 1983.

[10] S. Mohamed and T. Carrieres. Overview of new operational ice model. In *Proc. of* 9^{th} *International Offshore and Polar Engineering Conference*, pages 622–627, Brest, France, 1999.

[11] D. E. Nevel. The general solution of a wedge on a elastic foundation. *CRREL Research Report 227*, 1968.

[12] M. Sayed. and G. W. Timco. A lattice model of ice failure. In *Proc. of* 9^{th} *Int. Offshore and Polar Eng. Conf.*, pages 512–516, France, May 1999.

[13] G. W. Timco and M. Johnston. Ice loads on Caisson structures in the Canadian Beaufort Sea. *Cold Regions Science and Technology*, 38(2):185–189, 2004.